Electronic Supplementary Material (ESI) for Nanoscale.

Supporting Information

Tuning the electronic structure of $NiCoVO_x$ nanosheets through S doping for enhanced oxygen evolution

Haibin Ma,[‡,a] Changning Sun,[‡,a] Zhili Wang*[a] and Qing Jiang[a]

[a] Key Laboratory of Automobile Materials, Ministry of Education, and School of Materials Science and Engineering, Jilin University, Changchun 130022, China

*E-mail: zhiliwang@jlu.edu.cn

‡These authors contributed equally to this work.

Experimental Section

Chemicals

$Co(NO_3)_2 \cdot 6H_2O$, VCl_3, urea ($CO(NH_2)_2$), NH_4F, KOH, thiourea ($CS(NH_2)_2$), commercial IrO_2, isopropanol, nafion solution were purchased from China National Pharmaceutical Industry Corporation Ltd. NF was purchased from China Kunshan Yizhongtian New Material Corporation Ltd. Carbon paper (CC) was purchased from Taiwan Carbon Energy Technology Corporation Ltd. Deionized water (18.2 MΩ) was utilized in all the experimental procedures. All the reagents were of analytical grade and used as received without further treatment.

Material synthesis

Synthesis of $NiCoVO_x$/NF

$NiCoVO_x$/NF was obtained by the similar procedure as $S_{4.06}$-$NiCoVO_x$/NF without adding thiourea in the hydrothermal process.

Synthesis of S_m-$NiCoVO_x$/NF (m = 0.41, 2.89, 4.13, 6.26)

$S_{6.26}$-$NiCoVO_x$/NF, $S_{4.13}$-$NiCoVO_x$/NF, $S_{2.89}$-$NiCoVO_x$/NF, $S_{0.41}$-$NiCoVO_x$/NF samples were obtained from the similar procedure with $S_{4.06}$-$NiCoVO_x$/NF with some modifications. Typically, via tuning the atomic ratio of urea/thiourea into 1/4, 2/3, 3/2, 4/1, the resulting sample denoted as $S_{6.26}$-$NiCoVO_x$/NF, $S_{4.13}$-$NiCoVO_x$/NF, $S_{2.89}$-$NiCoVO_x$/NF, $S_{0.41}$-$NiCoVO_x$/NF, respectively, were obtained.

Synthesis of $S_{4.06}$-$NiCoVO_x$/CC and $S_{4.06}$-$CoVO_x$/CC

The $S_{4.06}$-$NiCoVO_x$/CC and $S_{4.06}$-$CoVO_x$/CC were prepared using the similar procedure as $S_{4.06}$-$NiCoVO_x$/NF except substituting NF with CC in the hydrothermal

process.

Preparation of IrO_2/NF

A total of 10 mg commercial powder IrO_2 was ultrasonically dispersed in 0.5 mL deionized water, 0.495 mL isopropanol, 0.05 mL of 5 wt% Nafion solution, then the ink was transferred onto a pre-treated NF electrode via a controlled drop casting method. The mass loading amount of IrO_2 kept the same with $S_{4.06}$-$NiCoVO_x$/NF sample.

Material characterizations

The morphology and structure of as-synthesis materials were investigated with scanning electron microscope (SEM). The atomic structure of samples was taken on transition electron microscope (TEM) with energy-dispersive X-ray spectroscopy (EDS) with a field emission gun operated at 200 kV. The thickness of nanosheets was measured by atomic force microscopy (AFM) (Bruker Dimension Icon, Germany). The X-ray diffraction data was obtained on a Bruker D8 Advance by X-ray diffractometer (Cu Kα radiation, λ=1.54178 Å). X-ray photoelectron spectroscopy (XPS) was collected with an Escalab 250 X-ray photoelectron spectroscope (15 kV, 6 mA). The energy scale was calibrated with C 1s spectrum at maximum peak of 284.8 eV as reference.

Computational Methods

All spin-polarized density functional theory plus Hubbard *U* (DFT+*U*) calculations were operated with the Vienna ab-initio simulation Package (VASP).[1] The exchange-correlation energy was described by using the generalized gradient

approximation (GGA) functional of Perdew-Burke-Ernzerhof (PBE)[2] and projected augmented wave (PAW)[3] pseudopotential. A plane-wave cutoff energy of 400 eV was adapt for all geometry optimization and energy calculation processes. Meanwhile, the energy and force convergence criteria of geometry optimization were 10^{-5} eV and 0.02 eV $Å^{-1}$, respectively. The first Brillouin zone was described by gamma centered *k*-points of 3×3×1 for geometry optimization and 7×7×1 for PDOS calculation. The solvent effect was considered by the implicit solvation method in $VASP_{sol}$ code.[4]

To describe V, Co and Ni 3*d*-electrons accurately, the Hubbard U_{eff*}(V)=3.25 eV, U_{eff*}(Co)=3.32 eV and U_{eff*}(Ni)=6.2 eV obtained from the Materials Project database[5] were added to the GGA functional of PBE via the rotationally invariant approach proposed by Dudarev *et al.*[6] Two 17.3 Å height 2×2 periodic slab models of $VNiO_3$ (220) and (020) plane with half of Ni replaced uniformly by Co were built as the substrates. A 15 Å vacuum space along the vertical direction was adopted to avoid the interactions between the slab and its period images. Moreover, a surface O atom nearing surface Co atom was substituted by S atom to study the effect of S doping. During all geometry optimization and energy calculation processes, the bottom half of atoms were fixed to their bulk positions, meanwhile the others were allowed to relax.

The computational hydrogen electrode (CHE) model was used to calculate the Gibbs free energy difference (ΔG),[7] which defined as:

$$\Delta G = \Delta E + \Delta ZPE - T\Delta S + \Delta G_U \quad (1)$$

where ΔE, ΔZPE and ΔS are the change of total energy, zero point energy, and entropy respectively, T is the temperature and ΔG_U is the contribution of potential

($\Delta G_U = -eU$). The OER process can be described by four electrochemical steps, they are

$$OH^-(aq)+*\rightarrow OH* \quad (2)$$

$$OH*+OH^-(aq)\rightarrow O*+H_2O(aq) \quad (3)$$

$$O*+OH^-(aq)\rightarrow OOH* \quad (4)$$

$$OOH*+OH^-(aq)\rightarrow OO*+H_2O(aq) \quad (5)$$

The four electrochemical steps correspond to four free energy changes, ΔGi (i=1,2,3,4), which determines the value of overpotential (η), defined as:

$$\eta=\max \Delta Gi/e-1.23V \quad (6)$$

where 1.23V is the equilibrium potential of OER.

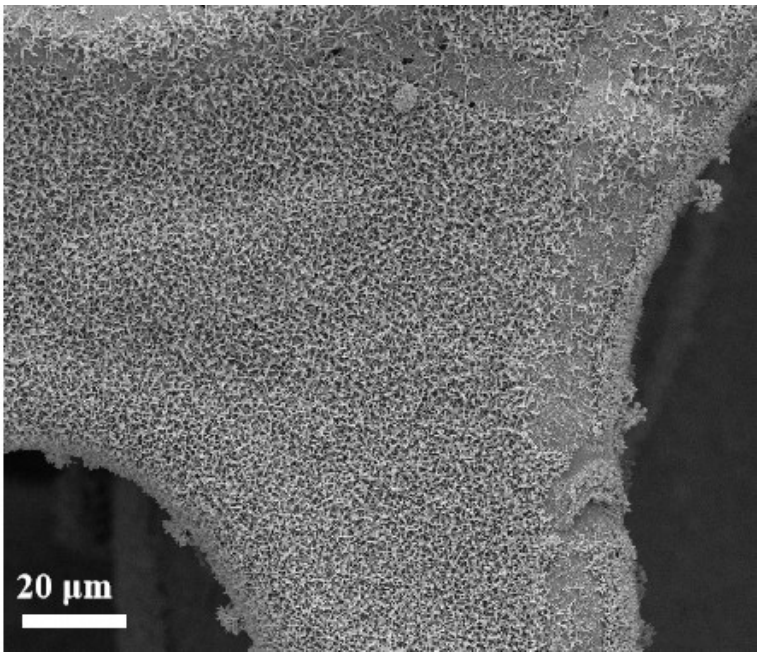

Fig. S1 SEM image of $S_{4.06}$-$NiCoVO_x$/NF.

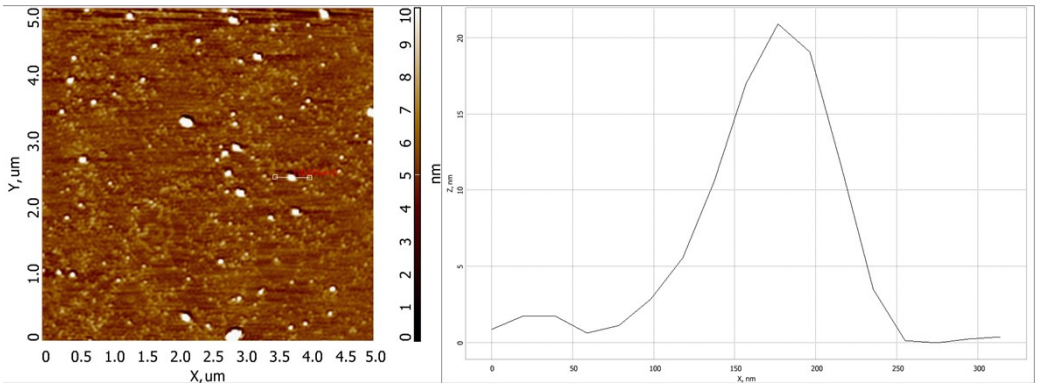

Fig. S2 Atomic force microscopy results for $S_{4.06}$-$NiCoVO_x$ nanosheets.

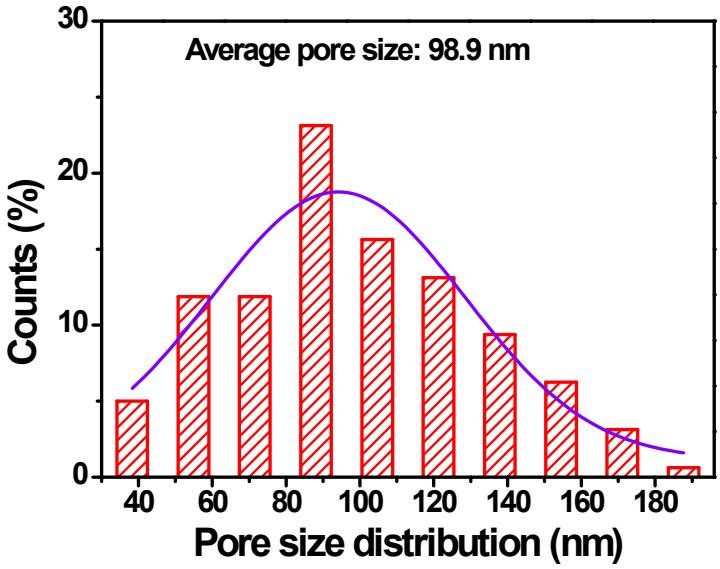

Fig. S3 Pore size distribution of the $S_{4.06}$-$NiCoVO_x$/NF.

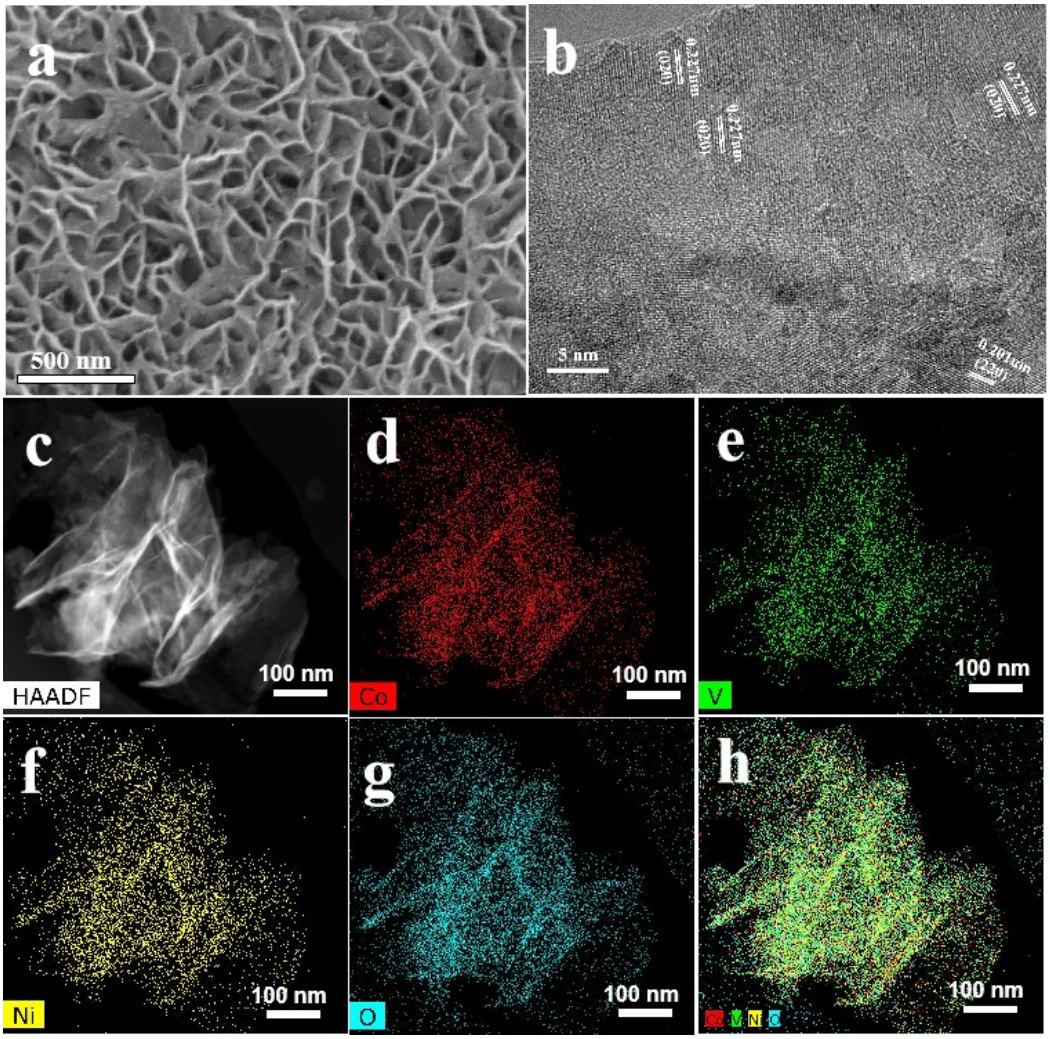

Fig. S4 (a) SEM and (b) HRTEM images of $NiCoVO_x$/NF. (c) HAADF-STEM image and the corresponding elemental mapping of $NiCoVO_x$ nanosheets.

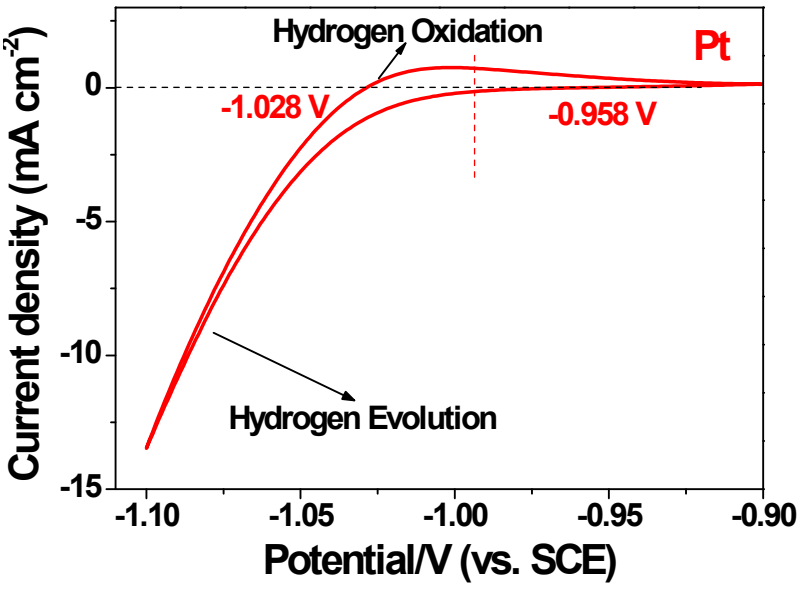

Fig. S5 RHE calibration in 1.0 M KOH, E(RHE) = E(SCE) + 0.993 V.

RHE calibration

The potential of calomel electrode was carefully calibrated with respect to the reversible hydrogen electrode. In detail, a calomel electrode (saturated KCl) was calibrated with respect to RHE in high purity hydrogen saturated 1.0 M KOH electrolyte with a Pt plate as the working electrode and platinum gauze as the counter electrode at a scan rate of 1 mV s^{-1}. The average of the two potentials at which the current crossed zero was taken to be the thermodynamic potential for the hydrogen electrode reaction.[8-9] The CV result was shown in Fig. S5. The potential reported in our work was converted to RHE according to the following equation: E(RHE) = E(SCE) + 0.993 V.

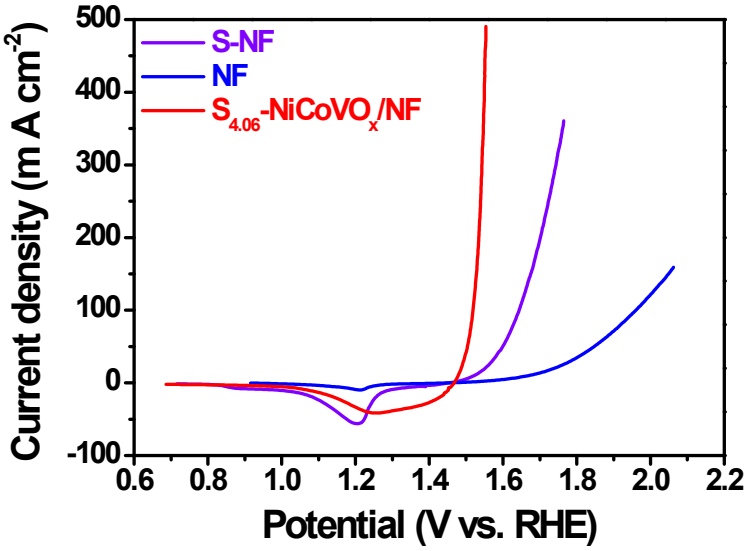

Fig. S6 LSV curves of NF, S-NF, and $S_{4.06}$-$NiCoVO_x$/NF. Sweep rate: 10 mV s^{-1}.

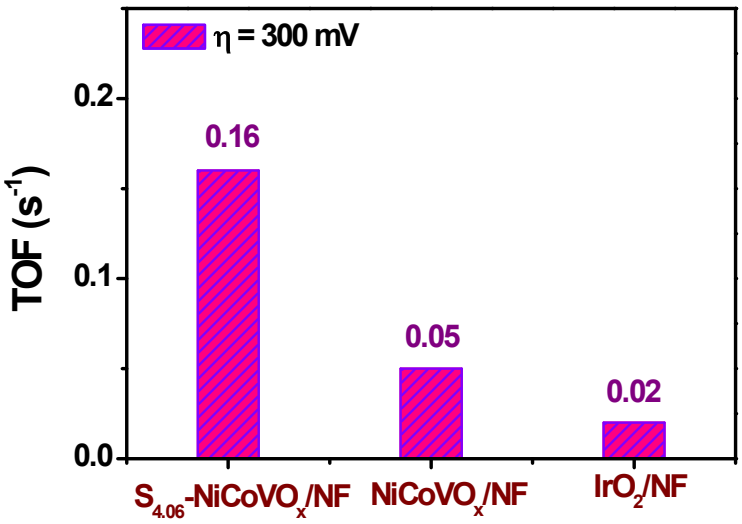

Fig. S7 Turnover frequency (TOF) of $S_{4.06}$-$NiCoVO_x$/NF, $NiCoVO_x$/NF and IrO_2/NF at the overpotential of 300 mV.

TOF was calculated according the equation as follow:[10]

$$TOF\ (s^{-1}) = (j \times A) / (4 \times F \times n)$$

Where j (A cm^{-2}) is the current density at overpotential of 300 mV, A (cm^2) is the area of NF, F is the Faradaic constant, the number 4 is the 4 electrons that were generated during OER process, and n is the moles of all metal species including Ni, Co and V loaded on NF.

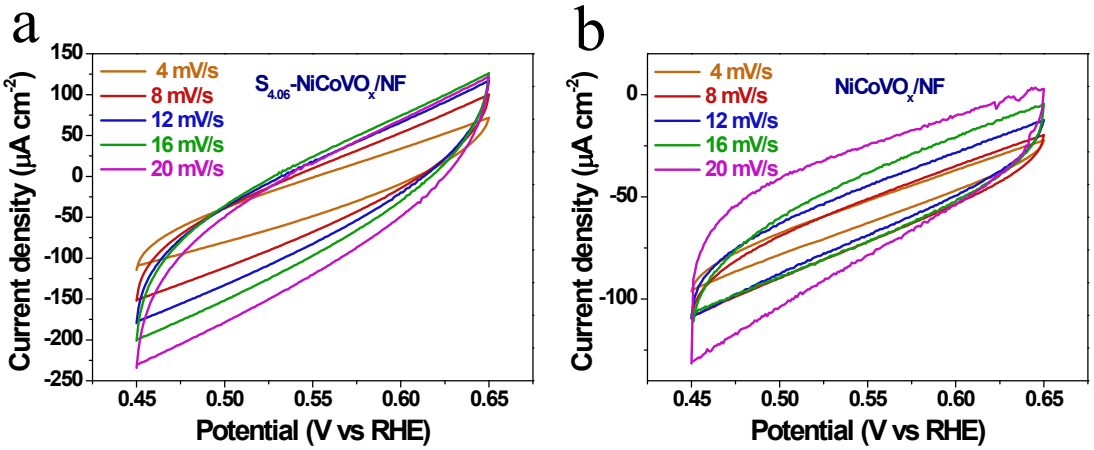

Fig. S8 The cyclic voltammograms at various scan rates of 4, 8, 12, 16, 20 mV/s for (a) $S_{4.06}$-$NiCoVO_x$/NF and (b) $NiCoVO_x$/NF.

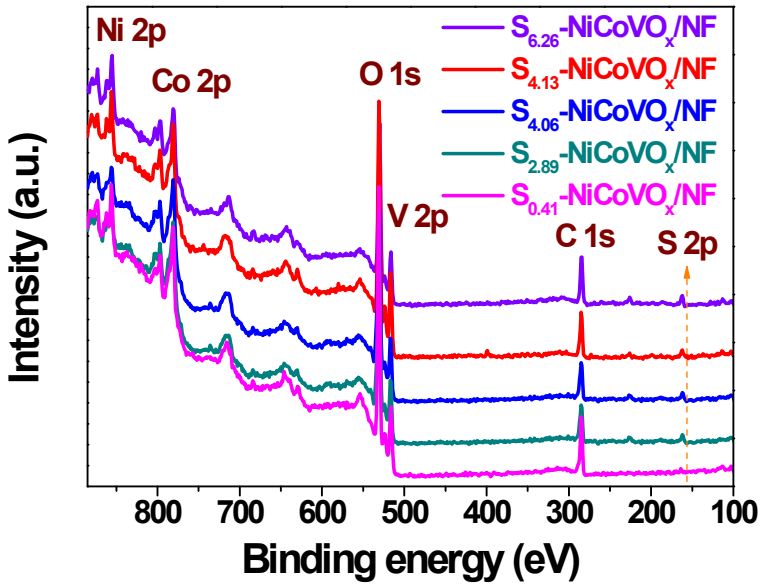

Fig. S9 XPS survey spectra of $S_{6.26}$-$NiCoVO_x$/NF, $S_{4.13}$-$NiCoVO_x$/NF, $S_{4.06}$-$NiCoVO_x$/NF, $S_{2.89}$-$NiCoVO_x$/NF and $S_{0.41}$-$NiCoVO_x$/NF.

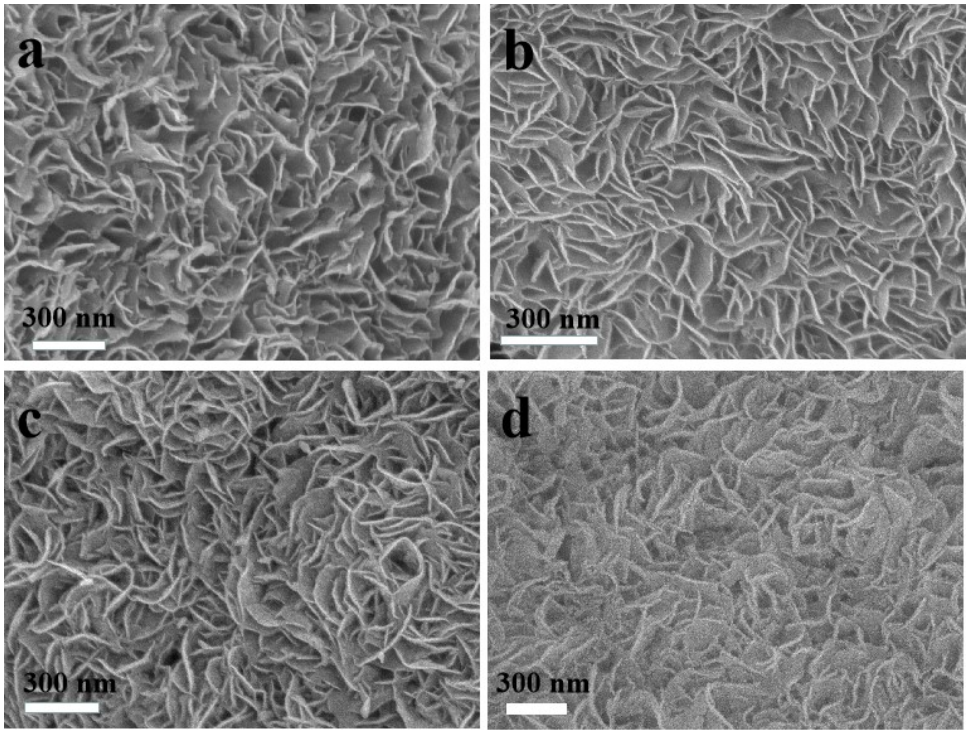

Fig. S10 SEM images of (a) $S_{6.26}$-$NiCoVO_x$/NF, (b) $S_{4.13}$-$NiCoVO_x$/NF, (c) $S_{2.89}$-$NiCoVO_x$/NF and (d) $S_{0.41}$-$NiCoVO_x$/NF.

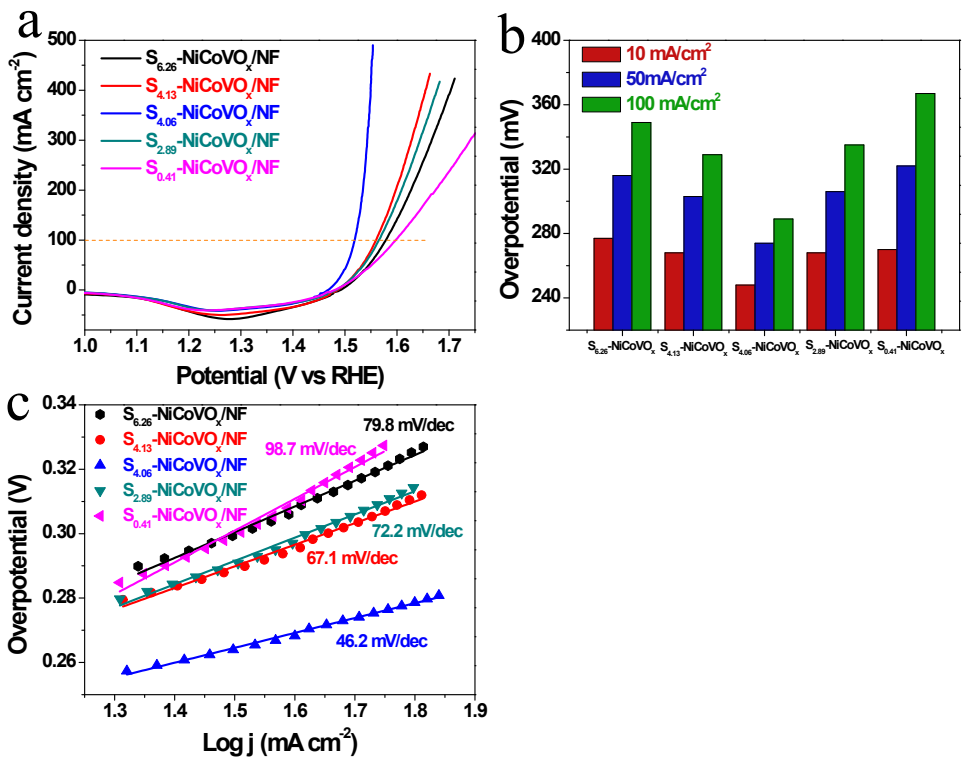

Fig. S11 OER activity tests of $S_{6.26}$-$NiCoVO_x$/NF, $S_{4.13}$-$NiCoVO_x$/NF, $S_{4.06}$-$NiCoVO_x$/NF, $S_{2.89}$-$NiCoVO_x$/NF and $S_{0.41}$-$NiCoVO_x$/NF. (a) LSV curves, (b) Tafel slopes of corresponding samples.

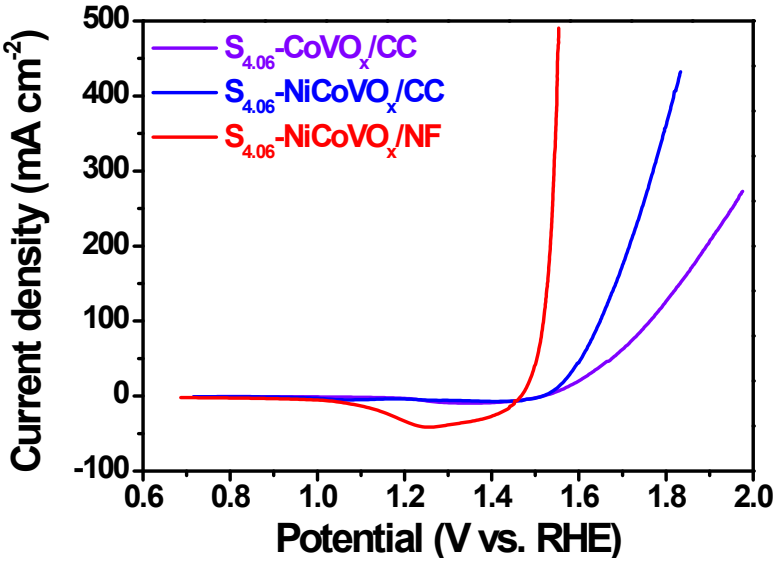

Fig. S12 LSV curves of $S_{4.06}$-$NiCoVO_x$/CC, $S_{4.06}$-$CoVO_x$/CC and $S_{4.06}$-$NiCoVO_x$/NF. Scan rate: 10 mV s^{-1}.

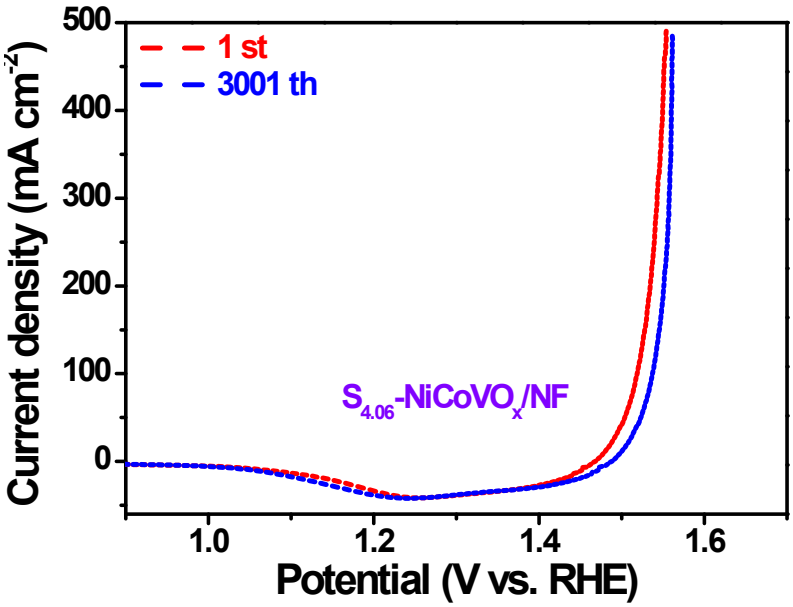

Fig. S13 LSV curves of $S_{4.06}$-$NiCoVO_x$/NF for 1st and 3001th cycle.

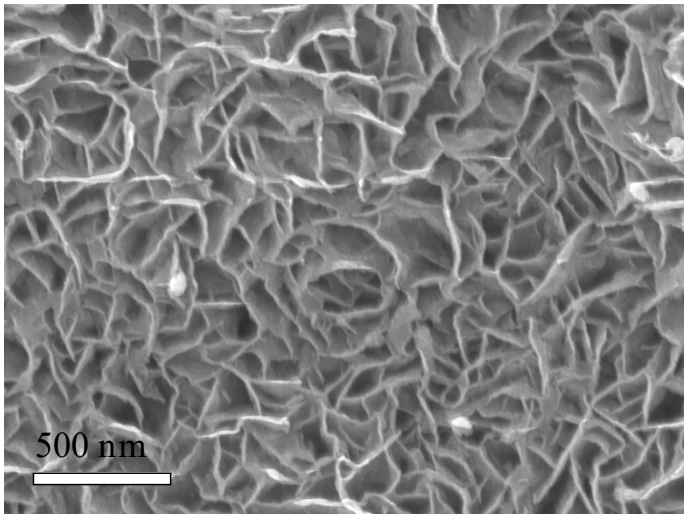

Fig. S14 SEM image of $S_{4.06}$-$NiCoVO_x$/NF after stability test.

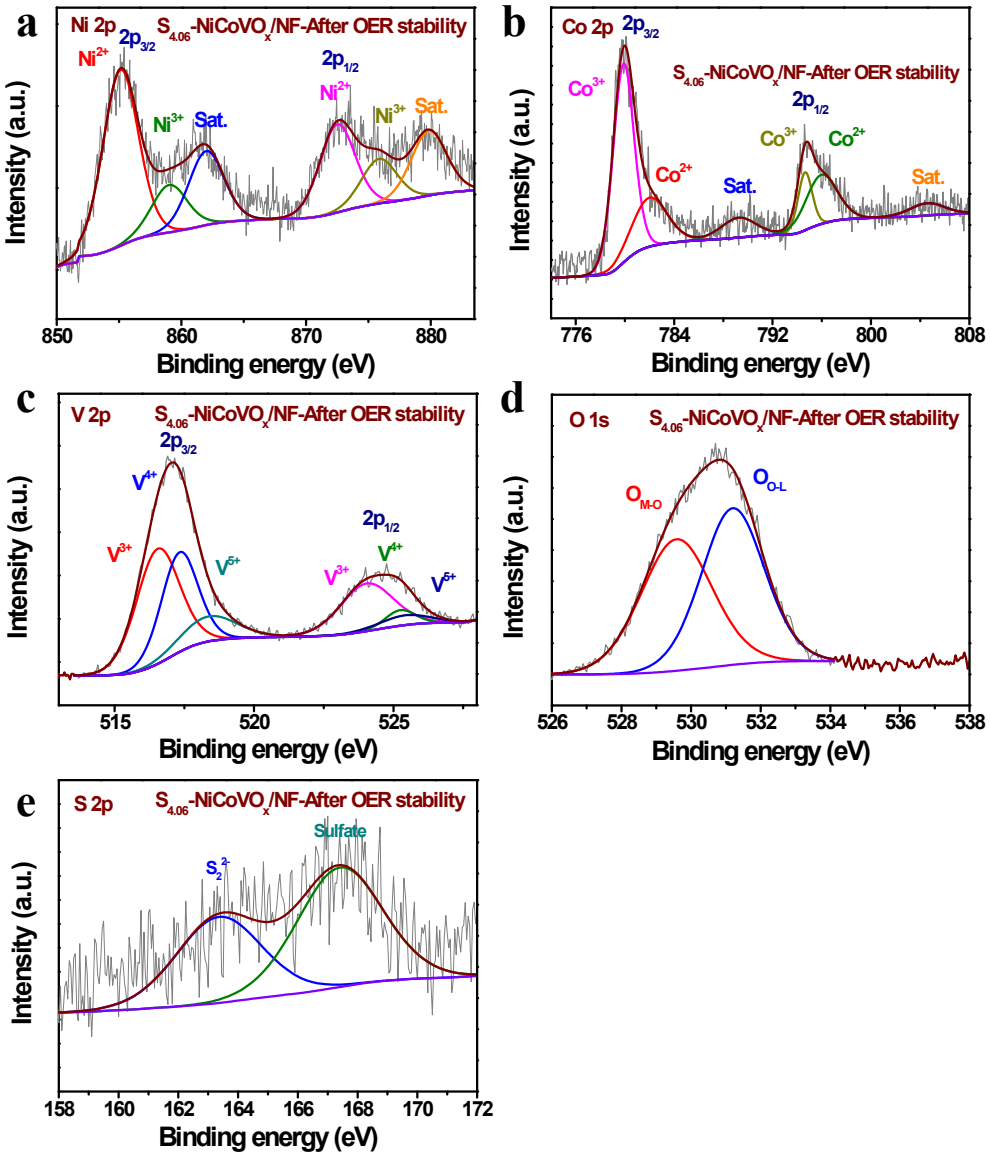

Fig. S15 High resolution XPS spectra of (a) Ni 2p, (b) Co 2p, (c) V 2p, (d) O 1s and (e) S 2p for $S_{4.06}$-$NiCoVO_x$/NF after stability test.

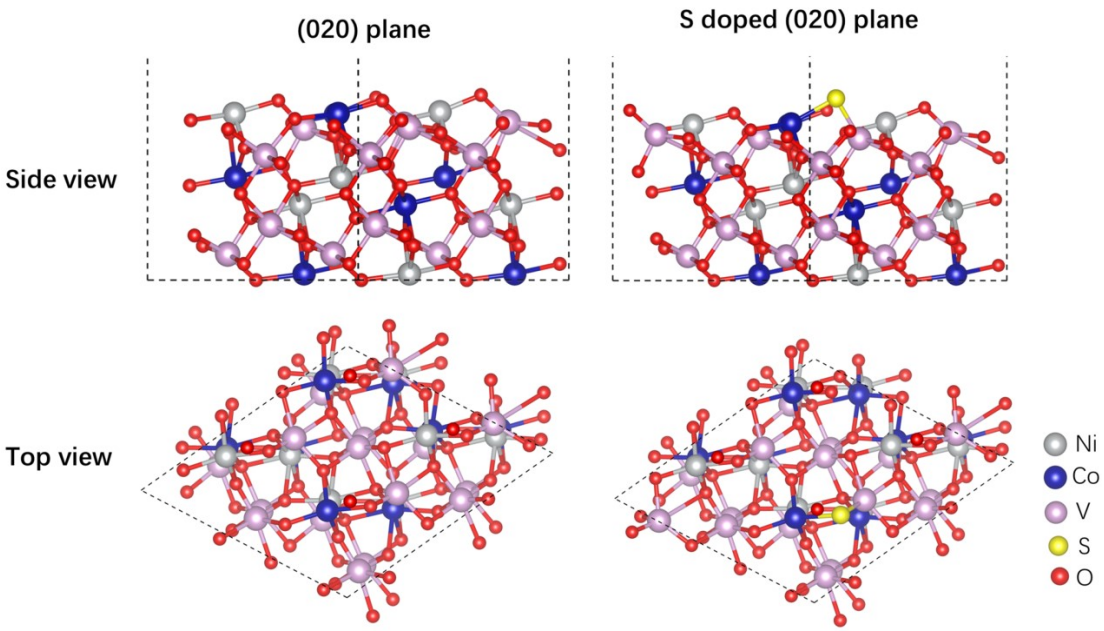

Fig. S16 The side and top views of $NiCoVO_3$ (020) plane before and after S doping.

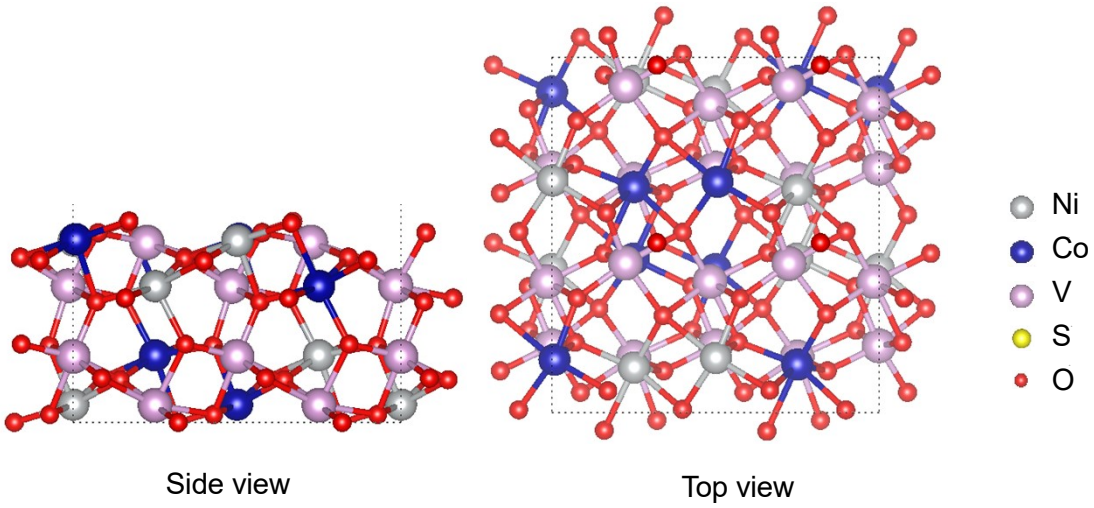

Fig. S17 The side and top views of $NiCoVO_3$ (220) plane.

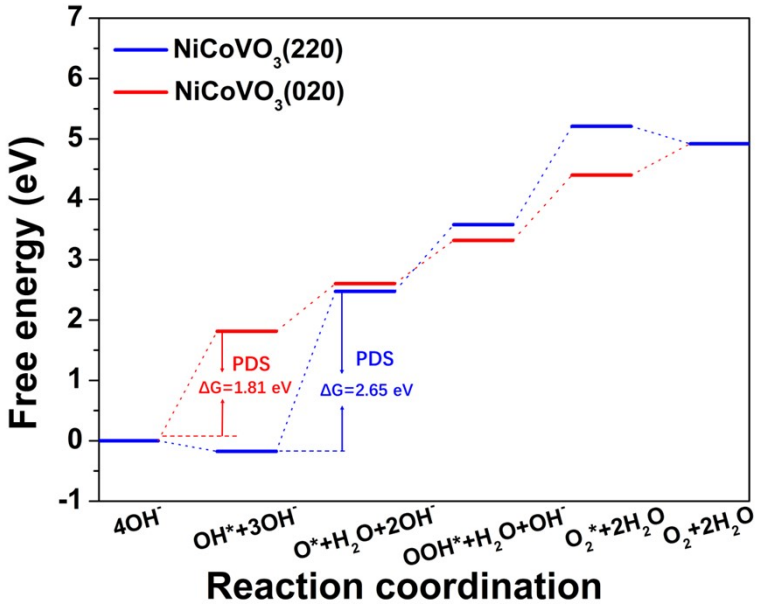

Fig. S18 The Gibbs free energy change diagram for OER pathway on bare $NiCoVO_3$ (220) and (020) plane.

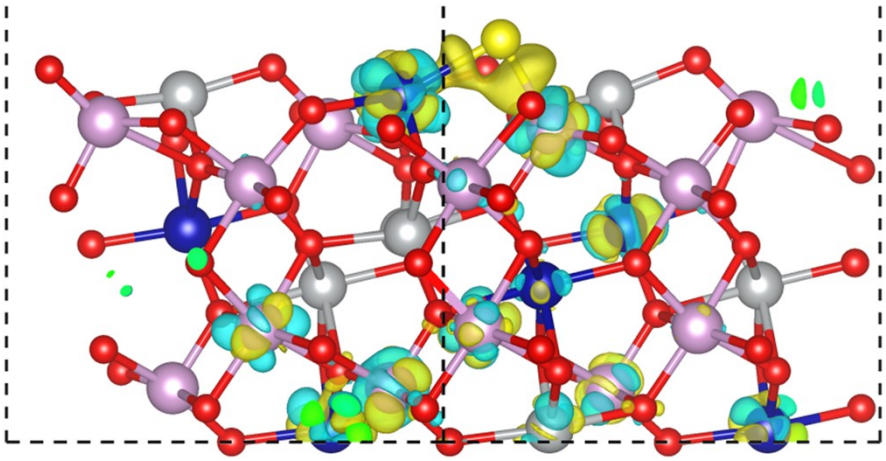

Fig. S19 The charge density difference of S-$NiCoVO_3$ (020) plane.

Table S1: Comparison of OER performance of $S_{4.06}$-$NiCoVO_x$/NF catalyst with recently reported non-noble metal based (hydro)oxides.

Catalyst	Electrolyte	Overpotential (mV)@10mA/ cm^2	Tafel Slope (mV/dec)	Reference
$S_{4.06}$-$NiCoVO_x$/NF	1 M KOH	248	46.2	*This work*
Fe-Co_3O_4	1 M KOH	262	43	11
CoV-$Fe_{0.28}$	1 M KOH	215	39.1	12
Ag/$Co(OH)_2$	1 M KOH	250	76	13
NiFeCr hydroxide/CeO_2/Cu	1 M KOH	230.8	32.7	14
CoFe-LDH	1 M KOH	320	53	15
$Fe_xCo_{1-x}OOH$	1 M KOH	266	30	16
Ir-doped $NiV(OH)_2$	1 M KOH	260	55.3	17
Gelled FeCo oxyhydroxides	1 M KOH	277	60	18
FeCoNi (oxy)hydroxide	1 M KOH	225	40.2	19
$Co_{0.75}Ni_{0.25}(OH)_2$	1 M KOH	235	56	20
$Co_{0.8}V_{0.2}OOH$	1 M KOH	190	39.6	21
CoFe-LDH-Ar	1 M KOH	266	37.9	22
Au@Co_3O_4 core-shell nanocrystals	1 M KOH	350	60	23
$FeCoO_x$	0.1 M KOH	400	48	24

Cobalt-vanadium (oxy)hydroxide	1 M KOH	250	44	25
CoO/Co_3O_4	1 M KOH	260	55	26
$Co_2Mo_3O_8$@NC-800	1 M KOH	331	87.5	27
Co_3O_4/CeO_2 NHs	1 M KOH	270	60	28
Co_3O_4/Co-Fe oxide DSNBs	1 M KOH	297	61	29
γ-CoOOH nanosheets	1M KOH	275	49	30
NiFeMo oxides	0.1 M KOH	280	49	31

References

1 K. G and F. J, *Comput. Mater. Sci.*, 1996, **6**, 15-50.

2 J. P. Perdew and W. Yue, *Phys. Rev. B Condens. Matter.*, 1986, **33**, 8800-8802.

3 P. E. Blochl, *Phys. Rev. B Condens. Matter.*, 1994, **50**, 17953-17979.

4 K. Mathew, R. Sundararaman, K. L. Weaver, T. A. Arias and R. G. Hennig, *J. Chem. Phys.*, 2014, **140**, 084106.

5 A. V. Krukau, O. A. Vydrov, A. F. Izmaylov and G. E. Scuseria, *J. Chem. Phys.*, 2006, **125**, 224106.

6 G. A. B. S. L. Dudarev, S. Y. Savrasov, C. J. Humphreys and A. P. Sutton, *Phys. Rev. B*, 1998, **57**, 1505-1509.

7 J. R. J. K. Nørskov, A. Logadottir and L. Lindqvist, *J. Phys. Chem. B*, 2004, **108**, 17886-17892.

8 H. Wang, Z. Chen, D. Wu, M. Cao, F. Sun, H. Zhang, H. You, W. Zhuang and R. Cao, *J. Am. Chem. Soc.* 2021, **143**, 4639–4645.

9 H. Shi, T. Y. Dai, W. B. Wan, Z. Wen, X. Y. Lang and Q. Jiang, *Adv. Funct. Mater.* 2021, 2102285.

10 J. Ge, R. R. Chen, X. Ren, J. Liu, S. J. H. Ong and Z. J. Xu, *Adv. Mater.* 2021, 2101091

11 S. L. Zhang, B. Y. Guan, X. F. Lu, S. Xi, Y. Du and X. W. Lou, *Adv. Mater.* 2020, 2002235.

12 M. Kuang, J. Zhang, D. Liu, H. Tan, K. N. Dinh, L. Yang, H. Ren, W. Huang, W. Fang, J. Yao, X. Hao, J. Xu, C. Liu, L. Song, B. Liu and Q. Yan, *Adv. Energy*

Mater. 2020, 2002215.

13 Z. Zhang, X. Li, C. Zhong, N. Zhao, Y. Deng, X. Han and W. Hu, *Angew. Chem., Int. Ed.* 2020, **59**, 7245-7250.

14 J. Xia, H. Zhao, B. Huang, L. Xu, M. Luo, J. Wang, F. Luo, Y. Du and C. H. Yan, *Adv. Funct. Mater.* 2020, **30**, 1908367.

15 Q. Zhou, Y. Chen, G. Zhao, Y. Lin, Z. Yu, X. Xu, X. Wang, H. K. Liu, W. Sun and S. X. Dou, *ACS Catal.* 2018, **8**, 5382-5390.

16 S. H. Ye, Z. X. Shi, J. X. Feng, Y. X. Tong and G. R. Li, *Angew. Chem., Int. Ed.* 2018, **57**, 2672-2676.

17 S. Li, C. Xi, Y. Z. Jin, D. Wu, J. Q. Wang, T. Liu, H. B. Wang, C. K. Dong, H. Liu, S. A. Kulinich and X. W. Du, *ACS Energy Lett.* 2019, **4**, 1823-1829.

18 B. Zhang, X. Zheng, O. Voznyy, R. Comin, M. Bajdich, M. G. Melchor, L. Han, J. Xu, M. Liu, L. Zheng, F. P. G. de Arquer, C. T. Dinh, F. Fan, M. Yuan, E. Yassitepe, N. Chen, T. Regier, P. Liu, Y. Li, P. D. Luna, A. Janmohamed, H. L. Xin, H. Yang, A. Vojvodic and E. H. Sargent, *Science* 2016, **352**, 333-337.

19 Q. Zhang, N. M. Bedford, J. Pan, X. Lu and R. Amal, *Adv. Energy Mater.* 2019, 1901312.

20 X. Wang, Z. Li, D. Y. Wu, G. R. Shen, C. Zou, Y. Feng, H. Liu, C. K. Dong and X. W. Du, *Small* 2019, **15**, 1804832.

21 Y. Cui, Y. Xue, R. Zhang, J. Zhang, X. Li and X. Zhu, *J. Mater. Chem. A.* 2019, **7**, 21911-21917.

22 Y. Wang, Y. Zhang, Z. Liu, C. Xie, S. Feng, D. Liu, M. Shao and S. Wang, *Angew.*

Chem., Int. Ed. 2017, **56**, 5867-5871.

23 Z. Zhuang, W. Sheng and Y. Yan, *Adv. Mater.* 2014, **26**, 3950-3955.

24 A. Indra, P. W. Menezes, N. R. Sahraie, A. Bergmann, C. Das, M. Tallarida, D. Schmeißer, P. Strasser and M. Driess, *J. Am. Chem. Soc.* 2014*,* **136**, 17530-17536.

25 J. Liu, Y. Ji, J. Nai, X. Niu, Y. Luo, L. Guo and S. Yang, *Energy Environ. Sci.* 2018, **11**, 1736-1741.

26 D. He, X. Song, W. Li, C. Tang, J. Liu, Z. Ke, C. Jiang and X. Xiao, *Angew. Chem., Int. Ed.* 2020, **59***,* 6929-6935.

27 T. Ouyang, X. T. Wang, X. Q. Mai, A. N. Chen, Z. Y. Tang and Z. Q. Liu, *Angew. Chem., Int. Ed.* 2020, **59**, 11948-11957.

28 Y. Liu, C. Ma, Q. Zhang, W. Wang, P. Pan, L. Gu, D. Xu, J. Bao and Z. Dai, *Adv. Mater.* 2019, **31***,*1900062.

29 X. Wang, L. Yu, B. Y. Guan, S. Song and X. W. Lou, *Adv. Mater.* 2018, **30***,*1801211.

30 H. Wang, E. Feng, Y. Liu and C. Zhang, *J. Mater. Chem. A.* 2019, **7**, 7777-7783.

31 Y. Duan, Z. Y. Yu, S. J. Hu, X. S. Zheng, C. T. Zhang, H. H. Ding, B. C. Hu, Q. Q. Fu, Z. L. Yu, X. Zheng, J. F. Zhu, M. R. Gao and S. H. Yu, *Angew. Chem., Int. Ed.* 2019, **58**, 15772-15777.